IEEE Access
Multidisciplinary | Rapid Review | Open Access Journal

Received June 3, 2020, accepted June 16, 2020, date of publication July 6, 2020, date of current version July 16, 2020.

Digital Object Identifier 10.1109/ACCESS.2020.3007339

Influence of a Novel Stator Teeth Internal Ventilation Structure on Air-Cooled Turbo-Generator Parameters and Stator Temperature

WENMAO LIU[1], (Graduate Student Member, IEEE), WEILI LI[1], (Member, IEEE), SHIFAN LUO[2], XUELIAN HUANG[3], DAN LI[1], (Graduate Student Member, IEEE), ZHIQIANG LI[4], (Member, IEEE), AND GUORUI XU[5], (Member, IEEE)

[1]School of Electrical Engineering, Beijing Jiaotong University, Beijing 100044, China
[2]College of Engineering, Northeastern University, Boston, MA 02115, USA
[3]Department of Electronic and Electrical Engineering, University of Strathclyde, Glasgow G1 1XQ, U.K.
[4]China Electric Power Research Institute Company Ltd., State Grid Corporation of China, Beijing 100192, China
[5]School of Electrical and Electronic Engineering, North China Electric Power University, Beijing 102206, China

Corresponding author: Weili Li (wlli@bjtu.edu.cn)

This work was supported by the National Natural Science Foundation of China under Grant 51477005 and Grant 51477049.

ABSTRACT In order to solve the problems of severe heating and cooling difficulty in the stator of air-cooled turbo-generator, a novel stator teeth internal ventilation structure with axial vents in the generator stator teeth is proposed. Based on this structure, global two-dimensional electromagnetic field models of 150MW air-cooled turbo-generator with different stator tooth internal ventilation structures are established to study the influence of the axial vents of the internal ventilation structure on air gap magnetic flux density of the generator, magnetic flux density of stator teeth, stator core loss, and synchronous reactance. Furtherly, flow network models of the ventilation system with different internal ventilation structures and fluid-heat transfer numerical models of stator with half axial and one tooth pitch of generator are established to calculate the effects of the structure on the temperature of stator winding, insulation and teeth. It can provide a new research idea for the ventilation structure of large air-cooled generator.

INDEX TERMS Air-cooled turbo-generator, ventilation structure, electromagnetic field, temperature field.

I. INTRODUCTION

The air-cooled turbo-generator does not require additional equipment for holding hydrogen and filtering water, compared with hydrogen-cooled and water-cooled turbo-generator. Therefore, the air-cooled turbo-generator is widely used in gas-steam combined cycle power station, and cogeneration for its advantages, energy conservation, environmental protection, safety and reliability [1]. With the continuous improvement of the generator unit capacity, the problems of severe heating and cooling difficulties become more and more serious. Especially the generator working in the operation of frequent start-stop and short-time overload, it will make the temperature of stator winding rise sharply. In severe cases, the generator stator windings and stator teeth are burned, when the cooling system is inefficient or failed. In order to improve the cooling capacity of the generator, this paper seeks an effective ventilation structure of stator on the basis of the traditional ventilation system of the air-cooled turbo-generator.

The research on the new structure of large-scale air-cooled turbo-generator ventilation system is less. Scholars have done the researches mainly on the optimization for the ventilation structure of generator. M. Fujita and other scholars proposed a method to reduce the ventilation volume and the ventilation loss by using variable pitch ventilation ducts in view of the high ventilation loss of air-cooled turbo-generator [2]. R. F. Gray proposed the optimization method for the cooling systems of the nuclear power turbo-generator with the largest capacity in the world at that time [3]. Georg proposed a calculation method for coupling the power loss, airflow and temperature of the air-cooled generator in an iterative

The associate editor coordinating the review of this manuscript and approving it for publication was Xiaokang Yin.

This work is licensed under a Creative Commons Attribution 4.0 License. For more information, see https://creativecommons.org/licenses/by/4.0/

process, and adjusted the cooling airflow to reduce ventilation loss [4]. M. Cheng proposed a robust fully forced-air cooling system with inner rotor tooth ducts for the dual mechanical port machine and designed a prototype of 10 kW air-cooled machine to verify the effectiveness of the cooling system [5]. J. Franc proposed ventilation system with skewed rotor cooling ducts of 40 MW synchronous turbo-generator, studied and compared the thermal behavior for three different arrangements of the rotor ventilation ducts, and pointed out the ways to improve the cooling system of the turbo-generator [6]. G. Zhou analyzed advantages and disadvantages of various ventilation systems for air-cooled turbo-generator, designed and optimized a multi-chamber forward-flow cooling path for a large air-cooled turbo-generator [7]. J. Nerg proposed a lumped-parameter-based thermal analysis of a generator with double radial forced-air cooling, and selected the number of radial cooling channels and axial length of the generator [8]. S. Ding established a global physical model including the stator, rotor, casing and fan to obtain air flow distribution characteristics of the generator under different ventilation schemes, and added the baffle at the rotor end to make the flow distribution more uniform and reasonable [9]. A. S. Bornschlegell used lumped-parameter method and genetic algorithm to calculate and optimize the air volume distribution in the ventilation system of a large generator [10]. W. Li changed the thickness of stator core stack segments and the number of radial ventilation ducts for 200 MW air-cooled turbo-generator to study the influence of different structures on the temperature field and coolant utilization ratio of the whole generator [11].

In this paper, the design idea of additional ventilation structure in stator teeth is proposed. However, the additional ventilation structure will result in local magnetic saturation of the stator tooth. This will change the magnetic circuit and magnetic flux density of the generator, and then affect he generator parameters. Therefore, it is particularly important to study the effect of new stator ventilation structure on air gap magnetic flux density, stator tooth magnetic flux density, synchronous reactance, stator core loss and the temperature of stator winding, insulation and teeth.

II. INFLUENCE OF STATOR TEETH INTERNAL VENTILATION STRUCTURE ON ELECTROMAGNETIC PARAMETERS

In this paper, a 150MW air-cooled turbo-generator with ventilation system of single centrifugal flow chamber path is presented for calculation and analysis. A circular vent with a diameter D_v is opened in each stator tooth portion at the position h_v along the each tooth centerline, and the vent penetrates the stator core along the axial direction z. This structure is called stator teeth internal ventilation structure (referred to as STIVS). The prototype and ventilation system are shown in Fig. 1. The stator core (DW310-50) and rotor core (25Cr2Ni4MoV) permeability are nonlinear. The nonlinearity of the magnetic properties is considered based on the actual B-H curve. The B-H curve of stator core and rotor core

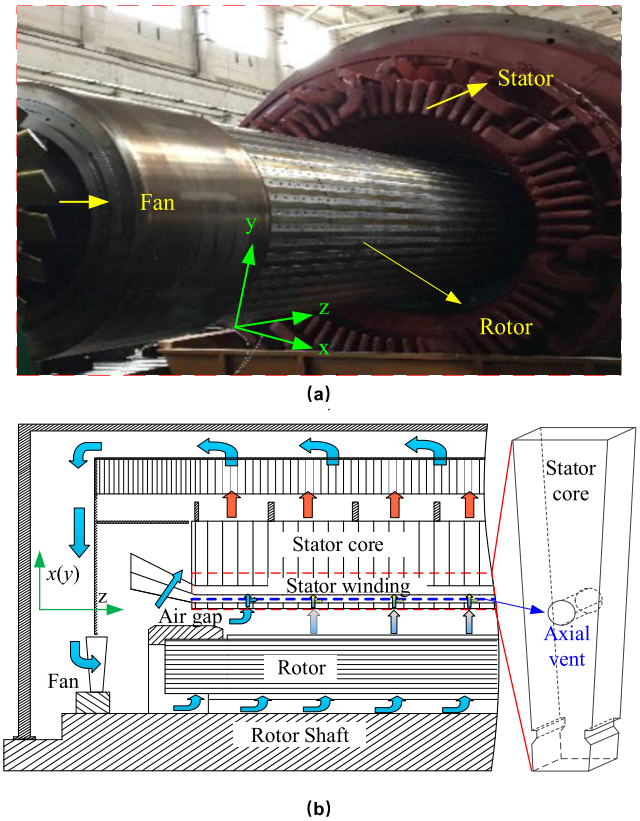

FIGURE 1. The prototype and ventilation system with STIVS(a)150MW air-cooled turbo-generator (b) Ventilation system.

are shown in Fig. 2, and the main parameters of the generator are given in Tab. 1.

TABLE 1. Basic parameters of 150MW generator.

Generator Parameter	Value
Rated Power(MW)	150
Rated Voltage(V)	15750
Rated Current(A)	6469
Rated Frequency(Hz)	50
Field Current (A)	1450
Stator Core Length (mm)	4200
Stator Core Stack Number	98
Radial Duct Width (mm)	7
Stator Slot Number	66
Stator Inner Diameter (mm)	1195
Stator Outer Diameter (mm)	2560
Rotor Inner Diameter (mm)	1060
Stator Tooth Depth (mm)	246
Stator Slot Width (mm)	26.3

A. ESTABLISHMENT OF 2-D ELECTROMAGNETIC FIELD MODELS OF GENERATOR WITH STIVSs

The axial length of the generator is 4200mm long, therefore, the internal magnetic field of the generator is a quasi-stationary field, and the magnetic field distribution in the axial position of the generator is consistent. Considering the

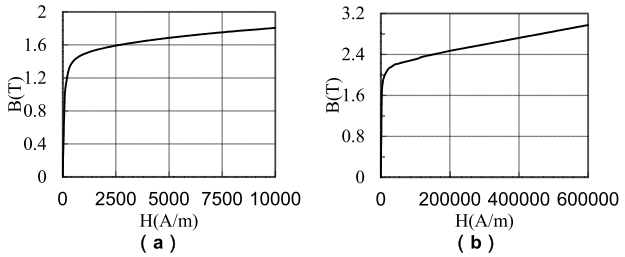

FIGURE 2. Armature equivalent circuit model (a) B-H magnetization curve for stator (b) B-H magnetization curve for rotor.

complexity and the massive computation of global three-dimensional (3-D) model of large turbo-generator, the 3-D space magnetic field is converted to the global 2-D magnetic field for analysis. For true calculation of the electromagnetic field, the global 2-D field-circuit coupling models of the generator with different STIVSs are established as shown in Fig. 3, where $r_{a,b,c}+jx_{\sigma a,b,c}$ are the three-phase winding resistance and end leakage reactance of the generator, and $R_{a,b,c}+jX_{a,b,c}$ are the equivalent rated load of the generator. And the excitation current and the rated load remain constant. In order to ensure the mechanical strength of the stator tooth, the diameter of the axial vent in the tooth should not be greater than 1/3 of the tooth width where it is located.

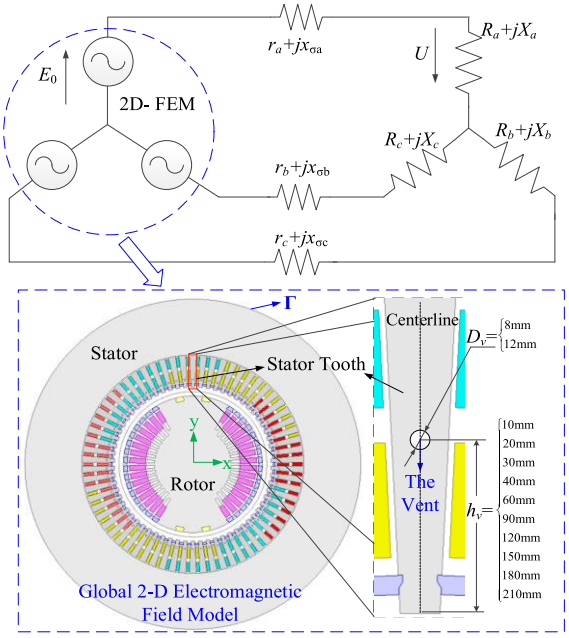

FIGURE 3. Global 2-D field-circuit coupling models of the generator with different STIVSs.

Before solving the model, we need to compute the rated field current of the generator iteratively and apply it to the rotor side of the model. The iterative calculation method is based on [12]. The calculation and measured values of field currents under no-load and rated-load are shown in Tab. 2.

Considering the magnetic saturation of stator core tooth, the boundary equation that satisfies the transient

TABLE 2. Calculation and measured values of field currents under no-load and rated-load.

No-load		Rated-load	
Calculation	Measurement	Calculation	Measurement
555 A	545 A	1450 A	1413 A

electromagnetic field equation is as follows [13]:

$$\begin{cases} \Omega : \dfrac{\partial}{\partial x}\left(\dfrac{1}{\mu}\cdot\dfrac{\partial \boldsymbol{A_Z}}{\partial x}\right)+\dfrac{\partial}{\partial y}\left(\dfrac{1}{\mu}\cdot\dfrac{\partial \boldsymbol{A_Z}}{\partial y}\right)=\boldsymbol{J_Z}+\sigma\dfrac{d\boldsymbol{A_Z}}{dt} \\ \Gamma : \boldsymbol{A_Z}=0 \end{cases} \quad (1)$$

where, $\boldsymbol{A_Z}$ is the magnetic vector potential (Wb/m) with only z axial component, $\boldsymbol{J_Z}$ is the source current density with only z axial component, σ is the electric conductivity (S/m), μ is the magnetic conductivity (H/m), t is time (s).

In order to improve the calculation accuracy to obtain the accurate values of magnetic flux density of the generator, the acute triangular elements are used in the model subdivision as far as possible. Small unit subdivisions are adopted at the corners and the junctions of tooth and slot, and multi-layer subdivisions are adopted in air gap, as shown in Fig. 4.

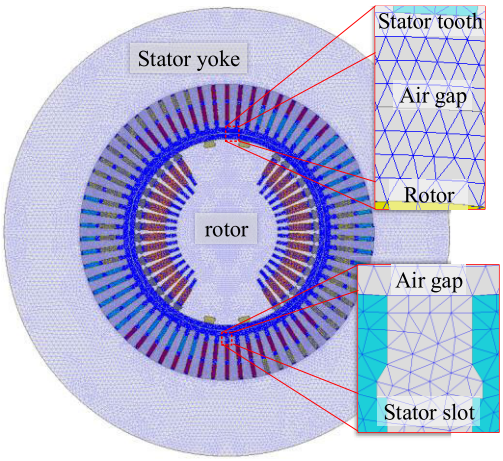

FIGURE 4. Detail subdivisions of the finite element calculation model.

B. EFFECTS OF STIVSs ON AIR GAP MAGNETIC FLUX DENSITY

After the calculation of the models, the influence of the axis vents on the harmonics of radial and tangential fundamental air gap magnetic flux density (AGMFD) are shown in Fig. 5. The changes of the harmonic amplitudes with different STIVSs are compared with the corresponding values of the original generator, as shown in Fig. 6. The amplitudes of 3rd, 5th, 7th, and 9th harmonics of the flux density of original generator are shown in Tab. 3.

It can be seen from Fig. 5 and 6 that the internal ventilation structure will reduce the radial fundamental AGMFD and 3rd harmonic, especially near the slot wedge and tooth top. The 5th, 7th, 9th harmonic increase at the slot wedge, but

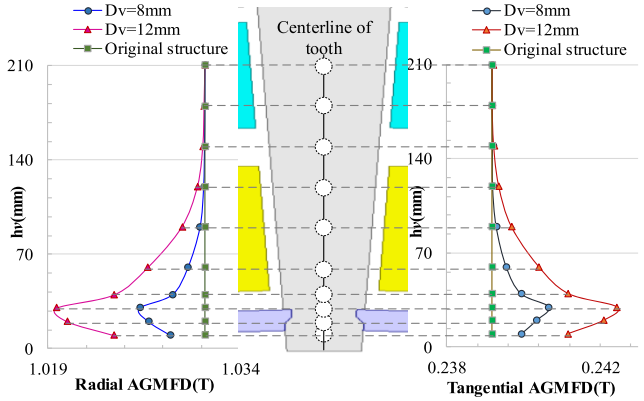

FIGURE 5. Influence of STIVS on the radial and tangential fundamental AGMFD.

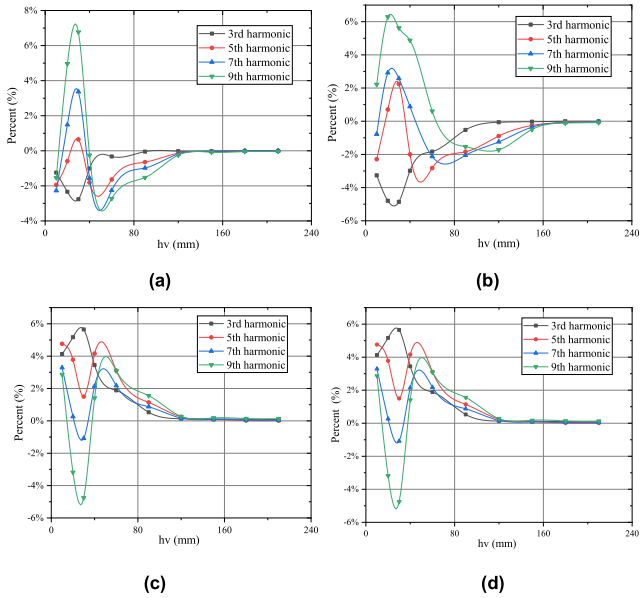

FIGURE 6. Influence of STIVS on the harmonics of tangential and radial AGMFD (a) Dv = 8mm, radial harmonic (b) Dv = 12mm, radial harmonic (c) Dv = 8mm, tangential harmonic (d) Dv = 12mm, tangential harmonic.

TABLE 3. The amplitudes of harmonics of the original generator.

Name	3rd	5th	7th	9th
Radial AGMFD	0.1138 T	0.0939 T	0.0483 T	0.0221 T
Tangential AGMFD	0.0231 T	0.0332 T	0.0374 T	0.0174 T

decrease at other positions. In contrast to the change of radial AGMFD, the structure will increase the tangential fundamental AGMFD and 3rd harmonic, especially near the slot wedge and the tooth top. The 5th, 7th and 9th harmonic decrease at the slot wedge, and increase at other positions. With the increase of h_v, the effect of the structure on the radial and tangential AGMFD is gradually weakened. Because when the internal ventilation structure is in the stator tooth, the tooth magnetic saturation will be deepened, and the magnetic resistance and the transverse magnetic flux leakage will be increased, which will affect the magnetic flux path and AGMFD of the generator. When the position of the internal ventilation structure is close to the tooth top and slot wedge, the influence is greater. Therefore, the STIVS with the minimal effect on the AGMFD should be selected.

C. EFFECTS OF STIVSs ON MAGNETIC FLUX DENSITY OF STATOR TEETH

Before studying the influence of the STIVS on the magnetic flux density of stator teeth, the average radial magnetic flux density of stator teeth of the original generator along the tooth is calculated, as shown in Fig. 7.

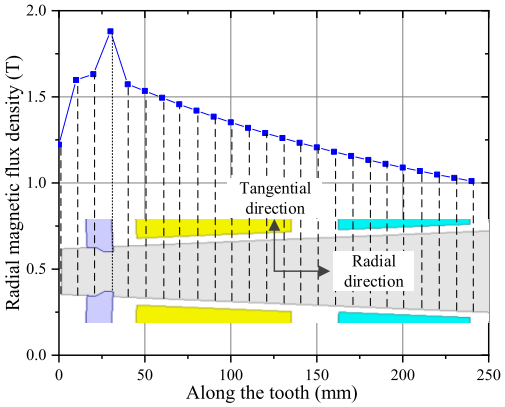

FIGURE 7. Variation of radial magnetic flux density of stator teeth of the original generator along the tooth.

As can be seen in Fig. 7, the radial magnetic flux density of stator teeth increases first and then decreases along the teeth. The value is larger at the stator slot wedge than that at the other positions. The tooth width at the tooth top is not much different from the tooth width near the slot wedge, but the difference in magnetic flux density is large. That's because when the main magnetic flux enters stator teeth through air gap, a part of the main magnetic flux will enter the teeth portion from the two sides of teeth wall near the teeth top. As a result, the radial magnetic flux density at the tooth top is smaller than that near the slot wedge.

Fig. 8 shows the variation of radial magnetic flux density along the tooth with the internal ventilation structures with different diameters D_v at different positions h_v.

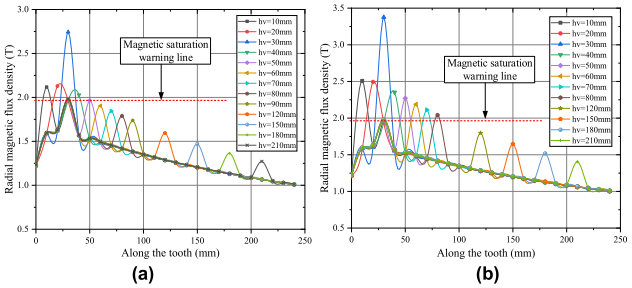

FIGURE 8. Effects of the ventilation structure on the radial magnetic flux density of stator teeth (a) Dv = 8 mm (b) Dv = 12 mm.

The STIVS causes magnetic oversaturation in the opening area of stator teeth. After the vent is opened, the position

of the maximum magnetic flux density is in the 20-40mm region. When D_v equals 8mm, the tooth magnetic flux density reaches 2.75T, which is 45% higher than that of the original structure. When D_v equals 12mm, the flux density reaches 3.4T, an increase of 83%, and reaches a severe degree of saturation. That has exceeded the normal test range of silicon steel sheet material. Here, the flux density is a calculated value, which is the product of the fitting magnetic permeability of the saturated region and the value of magnetic field strength. When the internal ventilation structure is in different positions of stator teeth, the local magnetic flux density increases to varying degrees. The rule is as follow that the magnetic flux density of stator teeth with new structure does not exceed the flux density of the original structure. Therefore, a magnetic saturation warning line is drawn in the Fig. 8. When the magnetic flux density is above the warning line, and the tooth is in magnetic oversaturation state, it is unsuitable to adopt such a structure.

D. EFFECTS OF T STIVSs ON STATOR CORE LOSS

The classical computational model for stator core loss proposed by Bertotti is used for the calculation, and its expression is [14]:

$$P_{Fe}=P_h+P_c+P_e=K_hfB_m^{\alpha}+K_cf^2B_m^2+K_ef^{1.5}B_m^{1.5} \quad (2)$$

where P_h is the hysteresis loss, P_c is the eddy current loss, P_e is the excess loss, B_m is the flux density amplitude, and K_h, K_c, and K_e are the corresponding loss coefficients.

The calculated stator core loss of the original structure is 220.2 kW, the measured value is 226.7 kW, and the error is within 3%. The influence of the internal ventilation structure on the stator core loss is shown in Fig. 9.

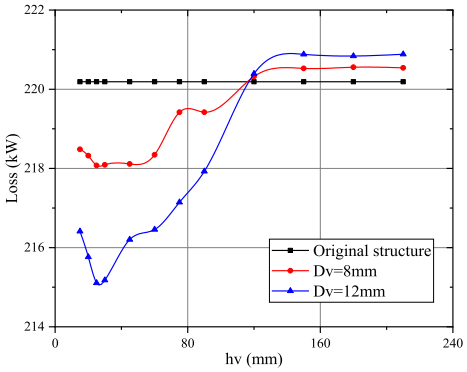

FIGURE 9. Influences of different STIVSs on stator core loss.

Compared with the stator core loss of the original structure, the loss decreases first and then increases with different position h_v. That's because when h_v is small, the axial vent locates where the magnetic flux density is large, and the core loss removed by opening axial vent accounts for a larger proportion of the total loss of core. Besides, when the axial vent is near the slot wedge and the tooth top, the flux leakage here increases, and the main magnetic flux entering the stator teeth decreases [15], resulting in a reduction in the magnetic flux density of stator teeth and a reduction in stator core loss. The narrower the tooth width is, the larger the vent diameter is, and the larger the change in stator core loss is. When the position h_v of the STIVS starts to be far away from the tooth top and slot wedge, the magnetic saturation degree of the tooth in the opening area is reduced, and the flux leakage is reduced, the effect on magnetic flux density of other areas is gradually reduced. According to (2), we know that the stator core loss is proportional to the first and second power of the stator magnetic flux density, so the stator core loss starts to increase until it is slightly larger than the loss of the original structure. The position h_v of the internal ventilation structure with the same stator core loss as the original structure is 100-130mm. When the STIVS is selected, the stator core loss should not be greater than that of the original generator.

E. EFFECTS OF STIVSs ON SYNCHRONOUS REACTANCE

Considering the stator leakage reactance, magnetic saturation and magnetic coupling between d-axis and q-axis of the generator, the load method [16] is used to calculate the synchronous reactance under rated load working conditions in this paper. The global 2-D static electromagnetic field models of the generator with different STIVSs are established, as shown in Fig. 10.

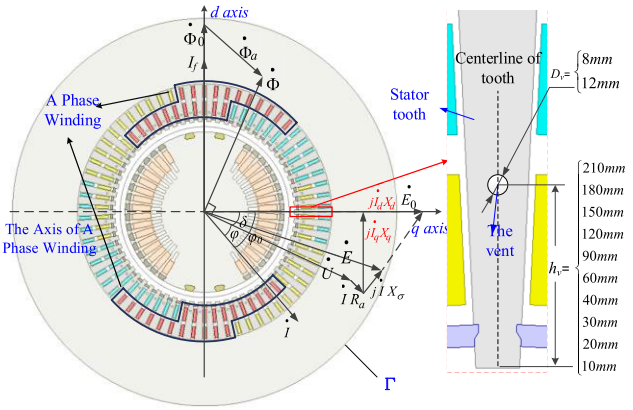

FIGURE 10. Phasor diagram of the synchronous reactance and global 2-D static electromagnetic field models with different internal ventilation structures.

The flux linkage equation in the *abc* coordinate system is calculated by the matrix equation:

$$\psi_{abc}=L_{abc}\cdot i_{abc} \quad (3)$$

where, L_{abc} is the inductance matrix of the three-phase winding, and i_{abc} is the current of the three-phase winding.

The inductance matrix L_{abc} obtained by solving (3) is transformed by the Park transformation to obtain inductance matrix L_{dq}, and is future calculated to obtain the X_{dq}:

$$X_{dq}=2\pi f\cdot L_{dq}=2\pi f\cdot C^TL_{abc}C \quad (4)$$

where C is the transformation matrix.

The calculated results of the synchronous reactance with different positions and diameters of the internal ventilation structure are shown in Fig. 11.

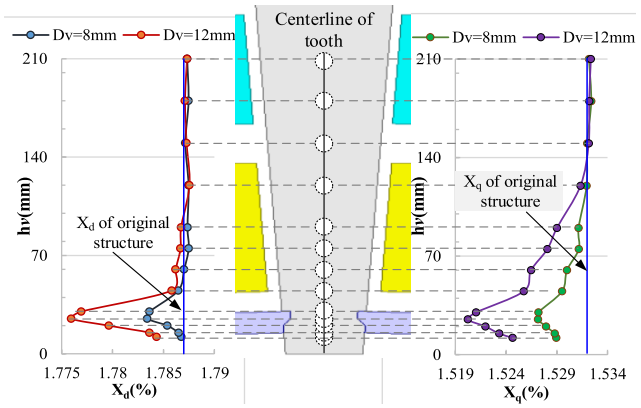

FIGURE 11. Effects of different STIVSs on synchronous reactance.

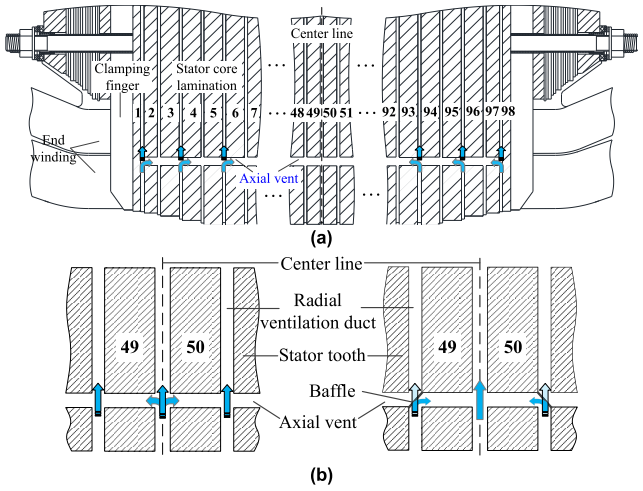

FIGURE 12. Axial vents of the STIVS in the stator core segments.

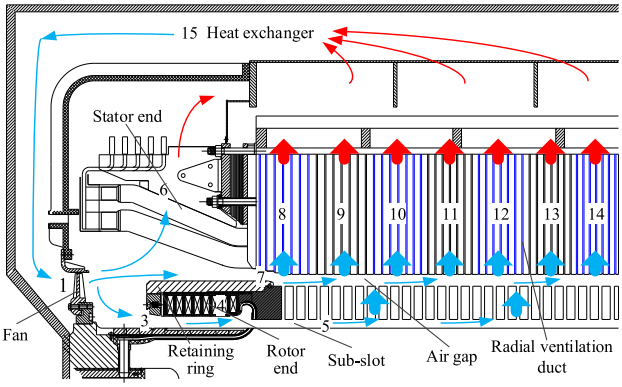

FIGURE 13. Ventilation system of single centrifugal flow chamber path.

As shown in Fig. 11, the reactance is slightly affected by the internal ventilation structure. With the changes of the position and diameter of the vent, the synchronous reactance still has a small variation trend, which is similar to the radial AGMFD. The opening vent in the area near the tooth top causes the tooth to be over magnetic saturated, increasing the leakage reactance [17] and making the main reactance decrease more, so the reactances X_d and X_q are reduced. The voltage regulation of the generator has a certain reduction. If the output voltage remains unchanged, the excitation current and loss would be slightly increased, and the generator efficiency and the material utilization rate will be reduced. Although the STIVS has little effect on the reactance as a whole, the structure with the least effect on reactance should be selected as far as possible.

III. INFLUENCE OF STATOR TEETH INTERNAL VENTILATION STRUCTURE ON VENTILATION SYSTEM OF THE GENERATOR

The ventilation system of single centrifugal flow chamber path of the 150MW air-cooled turbo-generator is taken as an example. This prototype has a total of 98 stator core stack segments. Except the outermost stator core stack segments at both ends, the axial vents are opened in the stator tooth portion from the excited end to the turbine end, that is, except No. 1 and No. 98 stator core stack segments, the other stator core teeth are provided with the axial vents, as shown in Fig. 12 a). Air-cooled turbo-generators have fans on both end sides. The air enters the air gap of the generator from both sides, and flows towards the center in the axial direction from the end. When the air flows towards the center, the air also flows into the stator radial ventilation duct, finally confluences at the central position of the generator and then enters the radial ventilation duct at the central position. With the flow and loss of air, the wind pressure of each radial ventilation duct of the stator is different. Because of the pressure difference, there is air flow in the axial vent connecting each radial ventilation duct. According to the axial symmetry of the ventilation system, the half axial ventilation system of the generator is taken as the research object, as shown in Fig. 13.

In order to simplify the system model, the on-way resistance is ignored, and the multiple parallel branches of the stator radial ventilation ducts in the flow network are combined for equivalent calculation.

The half axial ventilation system of the generator has 48 radial ventilation ducts. The thicknesses of core lamination from the generator end to the center include 42mm, 40mm, 35mm, and 30mm. In the establishment of flow network, the 48 ducts are divided into 7 groups. The parallel branches in the region of equal-thickness core lamination segments are equivalent to two branches. The parallel branches in the region of 30mm lamination are equivalent to one branch. The other branches of ventilation system are connected in reasonable series and parallel. The flow network model is established as shown in Fig. 14. 1 and 2 are the power source inside the ventilation network, which respectively represent the pressure head of the generator fan and centrifugal pressure of rotor; 3 to 15 are the resistance source of the network, which represent the wind resistances at key positions. Combined the fan external characteristics with the wind resistance characteristics of the ventilation system [18], the working point and the air volume in each region of the ventilation

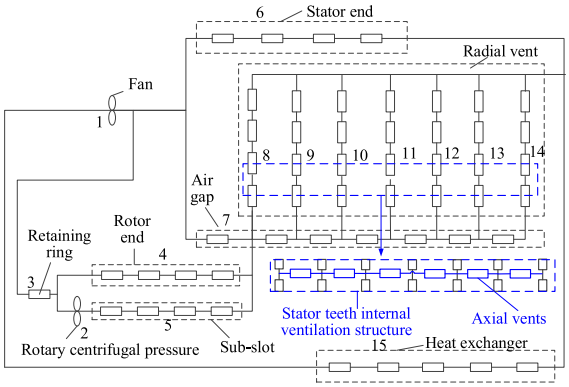

FIGURE 14. Flow network model of ventilation system of single centrifugal flow chamber path with stator teeth internal ventilation structure.

system can be calculated. The calculated and measured values are shown in Tab. 4.

TABLE 4. Calculated and measured values of air volume.

Name	Calculated values	Measured values
Total air volume (m^3/s)	46.04	43.6
Entrance of air gap (m^3/s)	30.46	—
Entrance of sub-slot (m^3/s)	11.22	—
Stator end (m^3/s)	4.36	—

The calculated value of the total air volume is 46m^3/s, the measured value is 43.6m^3/s, and the error is 5.5%. It verifies the accuracy of the flow network model.

A. WIND SPEED OF THE AXIAL VENTS IN DIFFERENT STIVSs

As can be seen from the previous studies, when h_v is between 90mm and 150mm, the influence of the internal ventilation structure on the electromagnetic parameters of the generator is little, and the influence on the efficiency and power of the generator can be approximately ignored. Therefore, the schemes of the internal ventilation structure, as shown in Tab. 5, are selected for further research. The corresponding flow network model with stator teeth internal ventilation structure is established, as shown in Fig. 14.

TABLE 5. Four schemes of the stator teeth internal ventilation structure.

Name	Scheme 1	Scheme 2	Scheme 3	Scheme 4
The diameter D_v	8 mm	12 mm	12 mm	12 mm
The position h_v	90 mm	90 mm	120 mm	150 mm

The wind speeds and pressures at key positions (end air gap inlet, stator yoke back outlet and rotor air gap outlet) are calculated by solving the established flow network models as boundary conditions of the 3-D fluid numerical models. The fluid numerical models are the half axial ventilation system with one tooth pitch of generator with the STIVSs, as shown in Fig. 15.

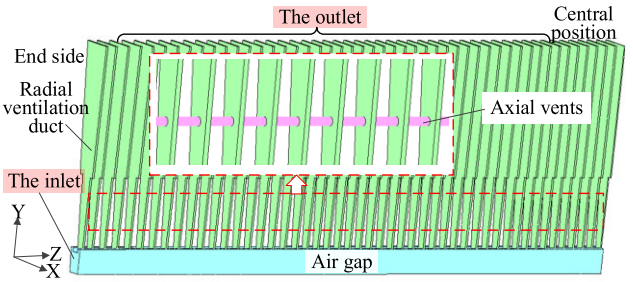

FIGURE 15. 3-D fluid solution domain model with stator teeth internal ventilation structure.

The boundary conditions are given in the model: (1) The inlet is the velocity inlet. (2) The outlet is the pressure outlet, setting as one atmosphere; (3) The outer surfaces of the fluid channel are no-slip boundaries.

The basic hypotheses are made in the model [19]: (1) The Reynolds number is large (Re>2320), and the turbulence model is adopted to solve the problem. (2) The influence of fluid buoyancy and gravity is without consideration. (3) The influence of rotor retaining ring on fluid flow at the air gap inlet is without consideration. (4) The fluid speed in the generator is much smaller than the sound speed, so the fluid is treated as an incompressible viscous fluid.

The standard k-ε turbulence equation is used to simulate and solve the fluid in the solution domain [20]:

$$\begin{cases} \dfrac{\partial(\rho k)}{\partial t} + \mathrm{div}(\rho k V) = \mathrm{div}\left[\left(\mu + \dfrac{\mu_t}{\sigma_k}\right)\mathrm{grad}k\right] \\ \qquad\qquad +G_k - \rho\varepsilon \\ \dfrac{\partial(\rho\varepsilon)}{\partial t} + \mathrm{div}(\rho V \varepsilon) = \mathrm{div}\left[\left(\mu + \dfrac{\mu_t}{\sigma_\varepsilon}\right)\mathrm{grad}\varepsilon\right] \\ \qquad\qquad +G_{1\varepsilon}\dfrac{\varepsilon}{k}G_k - G_{2\varepsilon}\rho\dfrac{\varepsilon^2}{k} \end{cases} \tag{5}$$

where, k is turbulent kinetic energy; ε is the diffusion factor; ρ is the fluid density; V is the velocity vector of the fluid; μ_t is turbulent viscosity; G_k is turbulence generation; $G_{1\varepsilon}$ and $G_{2\varepsilon}$ are constant; σ_k and σ_ε are turbulent Prandtl number.

Fig. 16 a) shows the average wind speed in the each axial vent of the STIVS under 1-4 schemes. The speeds of the vents

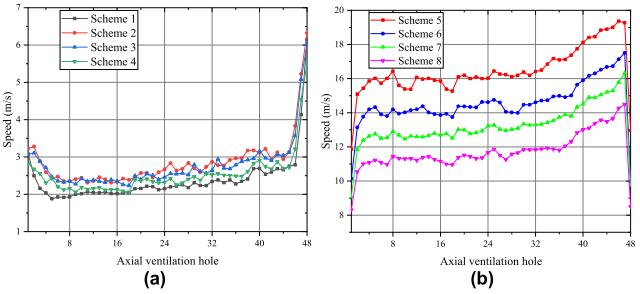

FIGURE 16. Average wind speed in the axial vents under different schemes (a) STIVSs without baffle (b) STIVSs with baffle.

are all small, because the pressure difference between two adjacent stator radial ventilation ducts in the ventilation system is small. The maximum speed in the axial vent is found near the generator center. Because when the air on both sides converges to the radial ventilation duct at the central position, the wind pressure here is larger than that of the adjacent radial ventilation ducts. The pressure difference between the two sides of the axial vent becomes large, so the wind speed in the axial vent here increases rapidly, and the reverse flow from the center to the two ends may occur, as shown in Fig.12 b).

B. EFFECTS OF STIVSs ON AIR VOLUME

Since the speeds in the axial vents of the 1-4 schemes are generally small, the baffle is considered to be located at the entrance of the axial vent to guide the cooling air into the vent, so as to make the stator tooth get more effective cooling. The structure and position of the baffle are shown in Fig. 17, and its width b is the same as the diameter D_v of the axial vent. The 5-8 schemes of the internal ventilation structures with baffle are shown in Tab. 6, and the established flow network model is shown in Fig.17.

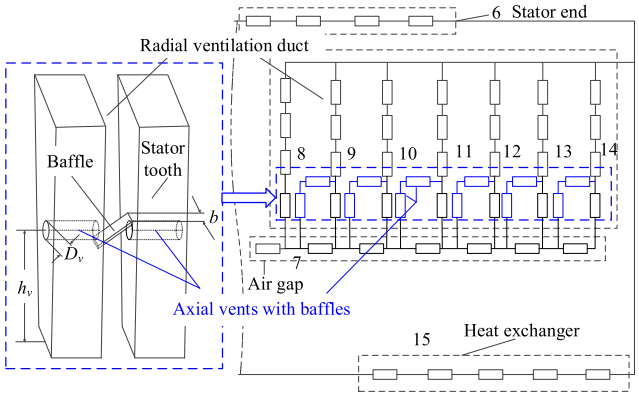

FIGURE 17. Flow network model of generator with the stator teeth internal ventilation structure and baffle.

TABLE 6. Four schemes of the stator tooth internal ventilation structure with baffle.

Name	Scheme 5	Scheme 6	Scheme 7	Scheme 8
The diameter D_v	8 mm	12 mm	12 mm	12 mm
The position h_v	90 mm	90 mm	120 mm	150 mm
The width b	8 mm	12 mm	12 mm	12 mm

The calculated results of the air volume of the 5-8 schemes are compared with that of the original generator, as shown in Tab. 7. We can see whatever scheme, it has little impact on the air volume of the generator. The results calculated by the model are taken as boundary conditions of the numerical model. The average speeds in each axial vent of the 5-8 schemes are obtained, as shown in Fig. 16 b). We can see that the closer the vent is to the generator center, the higher the wind speed is. The wind speed of the NO. 48 axial vent

TABLE 7. Calculation of wind volume for generator with stator tooth internal ventilation structure with baffle.

Name	Original structure	Scheme 5	Scheme 6	Scheme 7	Scheme 8
Total air volume (m^3/s)	46.04	45.75	45.6	45.68	45.82
Entrance of air gap (m^3/s)	30.46	30.12	29.94	30.06	30.2
Entrance of sub-slot (m^3/s)	11.22	11.2	11.18	11.19	11.2
Stator end (m^3/s)	4.36	4.43	4.48	4.43	4.42

decreases suddenly, because when the axial vents are added with deflectors, the air will be forced to flow from the two sides to the center. The flow direction of the axial vent at the central position is opposite to the direction of the previous wind pressure difference, besides, the air flow in the axial vent here has convection with air flow in the opposite axial vent, as shown in Figure 12. Therefore, the wind speed of the axial vent decreases rapidly here. Compared scheme 5 with 6, when the position of axial vent is the same, the smaller the vent size is, the higher the wind speed is. From schemes 6, 7 and 8, we can see that when the size of the vent is the same, the closer the vent is to the tooth top, the higher the wind speed is. Compared with the internal ventilation structure without the baffle, the average wind speed of the axial vent increases to 4-5 times.

IV. INFLUENCE OF STATOR TEETH INTERNAL VENTILATION STRUCTURE ON THE STATOR TEMPERATURE FIELD

A. ESTABLISHMENT OF STATOR 3-D FLUID-HEAT TRANSFER MODEL

Considering the symmetry of the ventilation system in both axial and circumferential directions of the generator, a 3-D fluid-heat transfer model of stator with half axial segment and one tooth pitch section of the generator is established, as shown in Fig. 18. The model includes a solid region and a fluid region. The solid region is composed of stator teeth with the STIVS, stator yoke, windings, slot wedges and insulation. The fluid region is composed of the air gap, stator radial ventilation ducts, and axial vents of the STIVS.

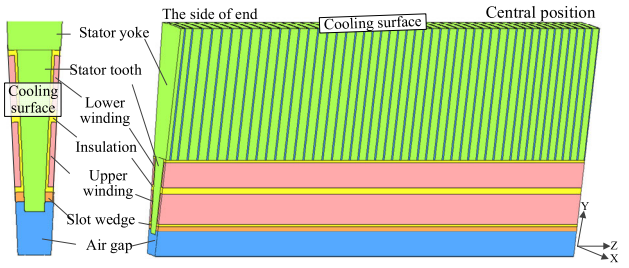

FIGURE 18. Stator 3-D fluid-heat transfer model.

In order to simplify the model calculation, additional assumptions are made in the model [21]: (1) The winding bar is considered as a whole. (2) The layer insulation is

considered as the main insulation. (3) The slot wedge is considered to have the same width as the stator slot. (4) The solids in this model have good contact with each other.

Besides the fluid boundary conditions, other conditions are given in the model [21]: (1) The heat sources in the model include the upper and lower winding, the stator tooth and yoke, and the air gap, and the heat source density is calculated by the average distribution. (2) According to the symmetry of the generator, the end surface of stator tooth, the surface of stator yoke, the back surface of the stator yoke and slot wedge surface are defined as the cooling surface. (3) The boundary surface of the solution domain is defined as the adiabatic surface except the outlet, inlet and the cooling surface above.

The fluid and temperature field of generator are calculated by finite volume method based on the fluid-heat transfer theory. In the model, the contact surfaces of solid and solid, solid and fluid all satisfy the 3-D heat transfer equation [21]:

$$\lambda_r \frac{1}{r}\frac{\partial}{\partial}\left(r\frac{\partial T}{\partial r}\right)+\lambda_\theta \frac{1}{r^2}\frac{\partial}{\partial}\left(r\frac{\partial T}{\partial \theta^2}\right)+\lambda_z \frac{\partial^2 T}{\partial z^2}+q=c\cdot\rho\frac{\partial T}{\partial t} \tag{6}$$

where λ_r, λ_θ and λ_z are the thermal conductivities respectively in the r, θ and z directions; q is heat density; T is the temperature; c is the specific heat capacity.

The finite volume method used in the calculation satisfies the mass conservation equation, momentum conservation equation and energy conservation equation [21]:

$$\begin{cases} \dfrac{\partial \rho}{\partial t}+\mathrm{div}\,(\rho v)=0 \\ \dfrac{\partial\,(\rho r)}{\partial t}+\mathrm{div}(\rho v_r)=\mathrm{div}\,(\mu\cdot \mathrm{grad} r)-\dfrac{\partial p}{\partial x}+S_r \\ \dfrac{\partial\,(\rho \theta)}{\partial t}+\mathrm{div}(\rho v_\theta)=\mathrm{div}\,(\mu\cdot \mathrm{grad}\theta)-\dfrac{\partial p}{\partial y}+S_\theta \\ \dfrac{\partial\,(\rho z)}{\partial t}+\mathrm{div}(\rho v_z)=\mathrm{div}\,(\mu\cdot \mathrm{grad} z)-\dfrac{\partial p}{\partial z}+S_Z \\ \dfrac{\partial\,(\rho T)}{\partial t}+\mathrm{div}\,(\rho v T)=\mathrm{div}\left(\dfrac{\lambda}{c}\mathrm{grad}T\right)+S_T \end{cases} \tag{7}$$

where, t is time; v is the velocity vector of the fluid; v_r, v_θ and v_z are the relative velocity vectors; P is the static pressure acting on the fluid element (Pa); μ is the viscosity coefficient; S_r, S_θ and S_z are the general source terms; S_T is the viscous dissipation.

The standard k-ε equation (7) is used to simulate the fluid.

B. CALCULATION AND ANALYSIS OF STATOR TEMPERATURE FIELD WITH STIVSs AND THE BAFFLE

The calculated temperature of the stator upper and lower winding of the original generator is shown in Fig. 19. The temperature increases from the end to the center. The highest temperatures of upper and lower winding are 129.2°C and 124.2°C, respectively. The prototype is manufactured and tested in a large generator equipment manufacturing plant. In order to more accurately measure the temperature of the stator windings, the stator bar is specially machined, and the

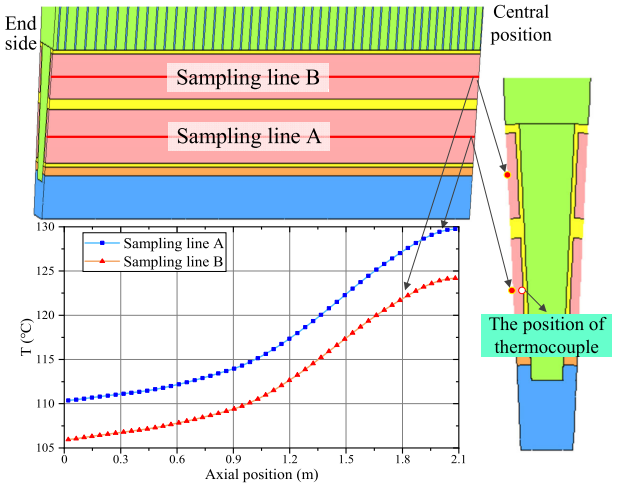

FIGURE 19. Sampling line temperature of upper and lower winding along z axis.

thermocouple is embedded in the stator's upper bar, close to the copper row, as shown in Fig. 19. The measured temperature is 123.7°C, which is a little different from the calculated value.

The ventilation structure runs through the stator tooth. When the air flows through the axial vents, the air will take away the heat of the stator tooth and directly cool the stator tooth. It will reduce the temperature of the winding insulation adjacent to the stator tooth, and accelerate the heat transfer from the winding to the insulation of the stator. Fig. 20 shows the stator winding temperature under 5-8 schemes. The STIVS reduces the stator windings temperature as a whole, and the overall reduction is 3-5°C. For the upper winding, scheme 6 has the best cooling effect, followed by scheme 7 and 5. For the lower winding, the cooling effects of scheme 7 and 8 are relatively better, followed by scheme 5 and 6. The axial vent of scheme 8 is close to the lower winding, but the average wind speed in the vent is low. It can't cool the lower winding better. The axial vent is far from the upper winding, and the cooling effect for the upper winding is insufficient.

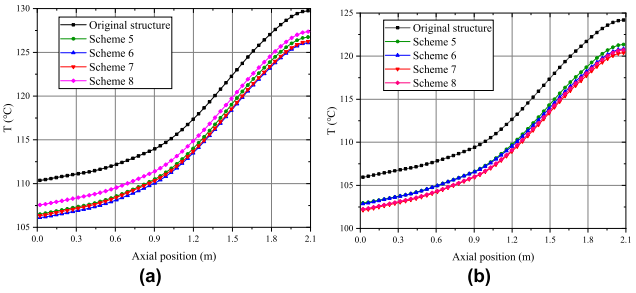

FIGURE 20. Influence of internal ventilation structure with baffle on the temperature of upper and lower windings along z axis (a) stator upper winding (b) stator lower winding.

Fig. 21 shows the temperature distributions of stator teeth on C-C' section along z axis, which is similar to that of the

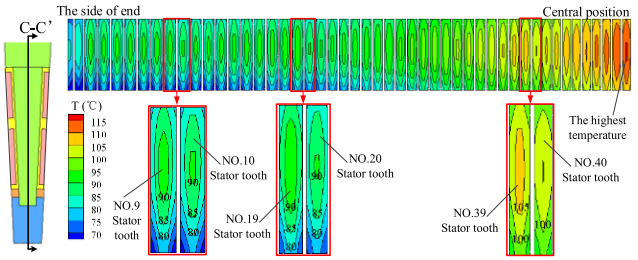

FIGURE 21. Temperature distributions of stator teeth on C-C′ section along z axis.

windings. However, the temperatures of No. 10, No. 20 and No. 40 stator teeth are slightly lower than those of the former ones, because the thicknesses of the core lamination are reduced from 42mm to 40mm, from 40mm to 35mm, and from 35mm to 30mm respectively. The cooling effects are relatively better than the former ones. The highest temperature of the stator tooth is about 116°C in the central region of generator and near the middle of stator teeth.

Fig. 22 shows the temperature distribution in the hottest region of the stator tooth under different schemes. We can see that the internal ventilation structure can effectively reduce the stator tooth temperature by about 3-4°C. From the results of scheme 5 and 6, it can be seen that when the structure position is the same, the larger the vent size is, the smaller the area of the high temperature zone is, and the better the cooling effect is. The maximum temperature of scheme 6 is 112°C, which is lower than 115°C of the original structure. The high temperature zone is significantly reduced from the range of 160-240mm to the range of 200-240mm. The maximum temperature of scheme 7 is 111°C, and the high temperature zone is divided into two parts by the axial vent. The maximum temperature of scheme 8 is 112 °C, and the high temperature zone becomes 140-200mm, moving down relative to the original zone. From schemes 6, 7 and 8, it can be seen that when the diameter of the axial vent is the same, the temperature, area and position of the high temperature zone are all changing with the variation of the axial vent position. The closer the vent is to the center of the tooth high temperature zone, the better the cooling effect is.

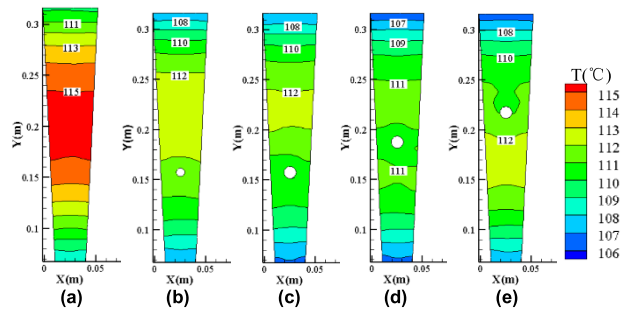

FIGURE 22. Temperature distributions in the hottest region of the stator tooth under different schemes (a) original structure (b) scheme 5 (c) scheme 6 (d) scheme 7 (e) scheme 8.

In Fig. 23, the blue sections 1-5 are sampling surfaces of the stator winding insulation. Fig. 23 shows the corresponding temperature distributions of the insulation along z axis, and the temperature in the hottest region of winding insulation with original structure and different schemes. We can see that the trend of the insulation temperature is the same as that of stator teeth. The highest temperature of the insulation is about 124°C near the generator center. The cooling effects of scheme 6 and 7 are better than those of scheme 5 and 8. The STIVS reduces the temperature of the insulation as a whole, and the overall reduction is about 4°C.

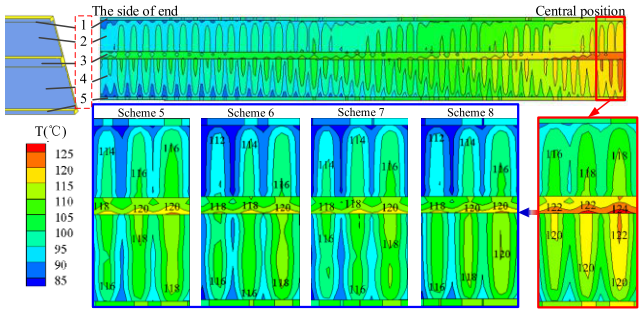

FIGURE 23. Temperature distributions in the hottest region of the winding insulation under original structure and different schemes.

V. CONCLUSION

In this paper, a novel stator teeth internal ventilation structure with axial vents in the generator stator is proposed. Based on this structure, 2-D electromagnetic field models of 150MW air-cooled turbo-generator, flow network models of the ventilation system and fluid-heat transfer models of stator are established to study the influence of the STIVS on electromagnetic parameters, fluid and temperature of generator. The beneficial conclusions are obtained:

1) The stator teeth internal ventilation structure increases the local magnetic saturation of stator teeth and the tangential flux density, reduces the radial air gap magnetic flux density and synchronous reactance, and first reduces and then increases the stator core loss from the tooth top to the root.
2) The closer the internal ventilation structure to the stator tooth top and slot wedge is, the greater the influence of the structure on the electromagnetic parameters is. The larger the diameter of the axial vent is, the greater the influence on the parameters is.
3) The internal ventilation structure has little effect on the air volume of the generator. The wind speed in the axial vent without the baffle is small, and the speed in the axial vent with the baffle increases to about 5 times larger than that without the baffle. The closer the internal ventilation structure to the stator tooth top is, the greater the wind speed in the axial vent is.
4) The internal ventilation structure can effectively reduce the temperature of stator windings, teeth and insulation by about 3-5°C. When the structure is located in the

high temperature zone of the stator tooth, the cooling effect is the best. When the vent diameter is larger, the cooling effect is better.

REFERENCES

[1] C. O. C. Oko and I. H. Njoku, "Performance analysis of an integrated gas-, steam- and organic fluid-cycle thermal power plant," *Energy*, vol. 122, pp. 431–443, Mar. 2017.
[2] M. Fujita, Y. Kabata, T. Tokumasu, M. Kakiuchi, H. Shiomi, and S. Nagano, "Air-cooled large turbine generator with multiple-pitched ventilation ducts," in *Proc. IEEE Int. Conf. Electr. Mach. Drives*, May 2005, pp. 910–917.
[3] R. F. Gray, L. Montgomery, R. Nelson, J. Pipkin, S. Joki-Korpel, and F. Caguiat, "Designing the cooling systems for the world's most powerful turbogenerator—Olkiluoto unit 3," in *Proc. IEEE Power Eng. Soc. Gen. Meeting*, Jun. 2006, p. 5.
[4] G. Traxler-Samek, R. Zickermann, and A. Schwery, "Cooling airflow, losses, and temperatures in large air-cooled synchronous machines," *IEEE Trans. Ind. Electron.*, vol. 57, no. 1, pp. 172–180, Jan. 2010.
[5] X. Sun and M. Cheng, "Thermal analysis and cooling system design of dual mechanical port machine for wind power application," *IEEE Trans. Ind. Electron.*, vol. 60, no. 5, pp. 1724–1733, May 2013.
[6] J. Franc, R. Pechanek, V. Kindl, and M. Zavrel, "Ventilation system with skewed rotor cooling ducts of 40-MW synchronous machine: A case study," *Electr. Eng.*, vol. 101, no. 1, pp. 203–211, Apr. 2019.
[7] G.-H. Zhou, L. Han, Z.-N. Fan, H.-B. Zhang, X.-C. Dong, J. Wang, Z. Sun, and B.-D. Zhang, "Ventilation cooling design for a novel 350-MW air-cooled turbo generator," *IEEE Access*, vol. 6, pp. 62184–62192, 2018.
[8] J. Nerg and V. Ruuskanen, "Lumped-parameter-based thermal analysis of a doubly radial forced-air-cooled direct-driven permanent magnet wind generator," *Math. Comput. Simul.*, vol. 90, pp. 218–229, Apr. 2013.
[9] S. Ding, X. Jiang, Z. Li, and Z. Li, "Research on relativity of flow rate distribution inside the rotor domain for a large-scale air-cooled turbo-generator," *IEEE Access*, vol. 7, pp. 174889–174897, 2019.
[10] A. S. Bornschlegell, J. Pelle, S. Harmand, A. Fasquelle, and J.-P. Corriou, "Thermal optimization of a high-power salient-pole electrical machine," *IEEE Trans. Ind. Electron.*, vol. 60, no. 5, pp. 1734–1746, May 2013.
[11] F. Huo, Y. Li, and W. Li, "Calculation and analysis on stator ventilation structure of different optimum proposal in air-cooled turbogenerator," *Proc. CSEE*, vol. 30, no. 6, pp. 69–75, Feb. 2010.
[12] L. Weili, G. Chunwei, and Z. Ping, "Calculation of a complex 3-D model of a turbogenerator with end region regarding electrical losses, cooling, and heating," *IEEE Trans. Energy Convers.*, vol. 26, no. 4, pp. 1073–1080, Dec. 2011.
[13] W. Yao, J.-M. Jin, P. T. Krein, and M. P. Magill, "A finite-element-based domain decomposition method for efficient simulation of nonlinear electromechanical problems," *IEEE Trans. Energy Convers.*, vol. 29, no. 2, pp. 309–319, Jun. 2014.
[14] G. Bertotti, "General properties of power losses in soft ferromagnetic materials," *IEEE Trans. Magn.*, vol. 24, no. 1, pp. 621–630, Jan. 1988.
[15] K. Shima, K. Ide, and M. Takahashi, "Analysis of leakage flux distributions in a salient-pole synchronous machine using finite elements," *IEEE Trans. Energy Convers.*, vol. 18, no. 1, pp. 63–70, Mar. 2003.
[16] R. Escarela-Perez, E. Campero-Littlewood, M. A. Arjona-Lopez, and A. Laureano-Cruces, "Comparison of two techniques for two-dimensional finite-element inductance computation of electrical machines," *IEE Proc.-Electr. Power Appl.*, vol. 152, no. 4, pp. 855–861, Jul. 2005.
[17] K. Shima, K. Ide, and M. Takahashi, "Finite-element calculation of leakage inductances of a saturated salient-pole synchronous machine with damper circuits," *IEEE Trans. Energy Convers.*, vol. 17, no. 4, pp. 463–470, Dec. 2002.
[18] S. Chen, "Network analyses of ventilation system for large hydrogenerator," in *Proc. 5th Int. Conf. Elect. Mach. Syst.*, vol. 1, Aug. 2001, pp. 137–140.
[19] J. Han, W. Li, L. Wang, X. Zhou, X. Zhang, and Y. Li, "Calculation and analysis of the surface heat-transfer coefficient and temperature fields on the three-dimensional complex end windings of a large turbogenerator," *IEEE Trans. Ind. Electron.*, vol. 61, no. 10, pp. 5222–5231, Oct. 2014.
[20] W. Li, X. Zhang, S. Cheng, and J. Cao, "Thermal optimization for a HSPMG used for distributed generation systems," *IEEE Trans. Ind. Electron.*, vol. 60, no. 2, pp. 474–482, Feb. 2013.
[21] J. Han, B. Ge, and W. Li, "Influence of magnetic permeability of the press plate on the loss and temperature of the end part in the end region of a turbogenerator," *IEEE Trans. Ind. Electron.*, vol. 66, no. 1, pp. 162–171, Jan. 2019.

WENMAO LIU (Graduate Student Member, IEEE) was born in Shandong, China, in 1988. He received the M.S. degree in power electronic and electrical drive from the Inner Mongolia University of Technology, Hohhot, China, in 2016. He is currently pursuing the Ph.D. degree in electrical engineering with the School of Electrical Engineering, Beijing Jiaotong University, Beijing, China.

His research interests include research on synthesis physical fields of large electrical machine, and the model and parameter of synchronous generator.

WEILI LI (Member, IEEE) was born in Harbin, China, in 1962. He received the M.S. degree in electrical machinery and appliance from the Harbin Institute of Electrical Technology, Harbin, in 1993, and the Ph.D. degree in electrical machinery and appliance from the Russia Electric Power Research Institute, Moscow, Russia, in 1997.

He is currently a Professor with the School of Electrical Engineering, Beijing Jiaotong University, Beijing, China. His research interests include research on synthesis physical fields of large electrical machine and special electrical machine.

SHIFAN LUO received the B.S. degree in electrical engineering from Miami University, OH, USA, in 2019. He is currently pursuing the degree in industrial engineering with Northeastern University, Boston, USA. His focus in M.S. education is in project management and data science.

In 2017, he joined the Redhawk Radio Station, Miami University, as the Chief Engineer, where he was responsible for maintain and update radio station hardware and software.

XUELIAN HUANG received the B.S. and M.S. degrees from the University of Strathclyde, Glasgow, U.K., in 2017 and 2019, respectively.

Her research interests include the modeling and analysis of HVDC transmission systems.

DAN LI (Graduate Student Member, IEEE) was born in Harbin, China, in 1990. She received the M.S. degree in electrical engineering from Beijing Jiaotong University, in 2017, where she is currently pursuing the Ph.D. degree in electrical engineering with the School of Electrical Engineering.

Her research interests include research on fluid field and temperature field of large electrical machine.

ZHIQIANG LI (Member, IEEE) was born in China, in 1978. He received the Ph.D. degree from North China Electric Power University, in 2009.

He is currently a Senior Engineer with the China Electric Power Research Institute. His research interests include power system modeling and parameters identification.

GUORUI XU (Member, IEEE) was born in Shanxi, China, in 1986. He received the B.E. degree from the Taiyuan University of Technology, Taiyuan, China, in 2007, and the M.E. and Ph.D. degrees in electric machines and apparatus from North China Electric Power University, Beijing, China, in 2010 and 2014, respectively.

He is currently an Associate Professor with North China Electric Power University. His research interests include synthesis physical field analyses on large synchronous generator and dual-excited synchronous generator, the model and parameter of synchronous generator, and coordination between units and grid.